Supporting Information

A dual-function Cd-MOF with high proton conduction and excellent fluorescence detection of pyridine

Guo-Mei Wu, [a] Ming-Yue Zhang, [b] Feng-Dong Wang, [a] Chen-Xi Zhang*[a] and Qing-Lun Wang*[c]

[a] *College of Chemical Engineering and Materials Science, Key Laboratory of Brine Chemical Engineering and Resource Eco-utilization, Tianjin University of Science and Technology, Tianjin 300457, P. R. China*

[b] *College of Sciences, Key Laboratory of Brine Chemical Engineering and Resource Eco-utilization, Tianjin University of Science and Technology, Tianjin 300457, P. R. China*

[c] *College of Chemistry, Key Laboratory of Advanced Energy Materials Chemistry (Ministry of Education), Nankai University, Tianjin 300071, P. R. China*

Materials and chemicals

The metal salts and organic solvents used in the experiment were commercially purchased reagents, which did not require further purification and could be used directly. The ligand 3,5-Diphosphonobenzoic Acid (H_5dpb) was synthesized according to the literature.[1] (Scheme 1 and Figure S20)

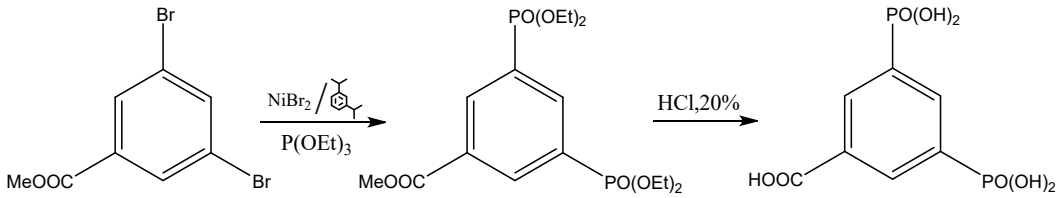

Scheme 1. Synthesis of 3,5-Diphosphonobenzoic Acid (H_5dpb).

Characterization

The FT-IR spectra were recorded on a Bruker Tensor 27 Fourier transform infrared spectrometer. ^{1}H NMR spectra of H_5dpb were performed on a Bruker AVANCE III at 400 MHz in D_2O. Elemental analyses for C and H were conducted on a Model 240 Perkin-Elmer analytical instrument. The powder X-ray diffraction (PXRD) measurements were acquired on a Shimadzu Labx XRD-6100 diffractometer with Cu K_α radiation (λ = 1.5418 Å). The intensity data were recorded by continuous scan in $2\theta/\theta$ mode from 5° to 50° at a scanning speed of 5° min^{-1} and a step size of 0.02°. Thermogravimetry analysis (TGA) was carried out using an SDT-Q600 instrument under a nitrogen atmosphere in the temperature range of 25-800 °C at a heating rate of 10 °C min^{-1}. The fluorescence test experiments were carried out on an F-280FL instrument. The prepared composite membranes were observed by a field emission SEM (JSM 6380LV) to obtain electron micrographs.

Table S1. Crystal data and structure refinement for Cd-MOF.

complex	Cd-MOF
Formula	$C_7H_{11}Cd_2O_{11}P_2$
Mr	557.81
T/K	293(2)
Crystal system	orthorhombic
Space group	*Pbcm*
***a*/ Å**	10.4801(3)
***b* / Å**	17.4762(5)
***c*/ Å**	7.0392(3)
***α* /°**	90
***β* /°**	90
***γ*/°**	90
Z	4
Volume /Å^3	1289.25(8)
***ρ* /g cm^{-3}**	2.854
***μ* /mm^{-1}**	3.606
***F*(000)**	1052.0
Crystal size /mm^3	0.22 × 0.18 × 0.16
***2θ* /°**	3.886 to 52.738
Reflections/ unique	9059/1422
$R_{(int)}$	0.1001
Data / restraints / parameters	1422/42/149
GOF on F^2	1.105
R_1 [I>2δ(I)]	0.0518
wR_2 [I>2δ(I)]	0.1705
R_1 (all data)	0.0525
wR_2 (all data)	0.1709

Table S2. Selected Bond Lengths (Å) and angles (°) of Cd-MOF.

Cd-MOF			
Cd(1)-O(2) #1	2.292(8)	Cd(2)-O(1)	2.284(13)
Cd(1)-O(3) #2	2.294(6)	Cd(2)-O(1) #5	2.284(13)
Cd(1)-O(3) #3	2.294(6)	Cd(2)-O(3)	2.358(5)
Cd(1)-O(6)	2.239(9)	Cd(2)-O(3) #5	2.358(5)
Cd(1)-O(7) #4	2.368(8)	Cd(2)-O(4) #6	2.208(15)
Cd(1)-O(8) #4	2.339(8)	Cd(2)-O(4) #7	2.208(15)
O(2) #1-Cd(1)-O(3) #2	85.67 (14)	O(1) #5-Cd(2)-O(1)	45.9(7)
O(2) #1-Cd(1)-O(3) #3	85.67(14)	O(1)-Cd(2)-O(3)	80.5(4)
O(2) #1-Cd(1)-O(7) #4	174.3(3)	O(1)-Cd(2)-O(3) #5	104.1(4)
O(2) #1-Cd(1)-O(8) #4	119.1(3)	O(1) #5-Cd(2)-O(3)	104.1(4)
O(3) #2-Cd(1)-O(3) #3	170.6(3)	O(1) #5-Cd(2)-O(3) #5	80.5(4)
O(3) #2-Cd(1)-O(7) #4	94.13(14)	O(3)-Cd(2)-O(3) #5	63.1(3)
O(2) #3-Cd(1)-O(7) #4	94.13(14)	O(4) #7-Cd(2)-O(3)	149.5(5)
O(3) #3-Cd(1)-O(8) #4	90.48 (13)	O(4) #7-Cd(2)-O(3) #5	100.1(5)
O(3) #2-Cd(1)-O(8) #4	90.48 (13)	O(4) #6-Cd(2)-O(3) #5	149.5(5)
O(6)-Cd(1)-O(2) #1	99.8 (3)	O(4) #6-Cd(2)-O(3)	100.1(5)
O(6)-Cd(1)-O(3) #3	92.57(14)	O(4) #6-Cd(2)-O(4) #7	82.1(9)
O(6)-Cd(1)-O(3) #2	92.57(14)	Cd(1) #2-O(3)-Cd(2)	121.1(2)
O(6)-Cd(1)-O(7) #4	85.9(3)		
O(6)-Cd(1)-O(8) #4	141.1(3)		
O(8) #4-Cd(1)-O(7) #4	55.2(3)		

Symmetry Codes: #1 = 1+X,+Y,+Z; #2 = 1-X,1-Y,-1/2+Z; #3 = 1-X,1-Y,2-Z; #4 = 1-X,1/2+Y,3/2-Z; #5 = +X,+Y,3/2-Z; #6 = 1-X,1-Y,1/2+Z; #7 = 1-X,1-Y,1-Z

Table S3. Hydrogen bond Lengths (Å) and Angles (°) for Cd-MOF.

D-H⋯A	d(D-H)	d(H⋯A)	d(D⋯A)	<(D-H⋯A)
O(5)-H(5A)⋯O(2)	0.86	1.79	2.645	178
O(6)-H(6A)⋯O(5)	0.861	1.888	2.748	178
O(6)-H(6B)⋯O(3)	0.86	1.94	2.781	168
O(7)-H(7A)⋯O(8)	0.86	2.18	2.947	149
O(7)-H(7A)⋯O(4)	0.86	2.46	3.103	132
O(7)-H(7A)⋯O(3)	0.86	1.98	2.790	157
O(8)-H(8A)⋯O(1)	0.86	1.89	2.719	161
O(8)-H(8B)⋯O(4)	0.856	2.076	2.870	154

Table S4. The proton conductivities value of Cd-MOF@CS-X composite membranes in comparison with other MOFs composite materials.

Materials	σ/S cm^{-1}	Conditions	References
Cd-MOF@CS-5	3.55×10^{-1}	353 K, 98% RH	This work
PSS@ZIF-8	2.59×10^{-1}	353 K, 100% RH	2
MNFs@SPES-7	2.48×10^{-1}	353 K, 100% RH	3
DNA@ZIF-8-3/25	1.70×10^{-1}	348 K, 97% RH	4
BUT8(Cr)A	1.27×10^{-1}	353 K, 100% RH	5
CS/H_2SO_4@MIL-101-8	9.50×10^{-2}	373K, 100% RH	6
CS/H_3PO_4@MIL-101-6	8.30×10^{-2}	373K, 100% RH	6
Im@MOF-808	3.45×10^{-2}	338K, 99% RH	7
CS/A + B	5.20×10^{-2}	373 K, 98% RH	8

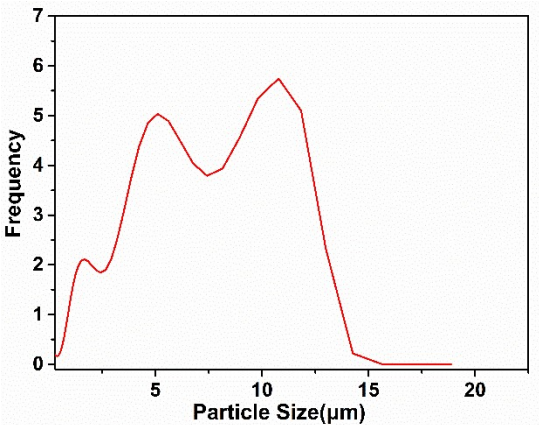

Figure S1. Particle size distribution of Cd-MOF dispersed in deionized water.

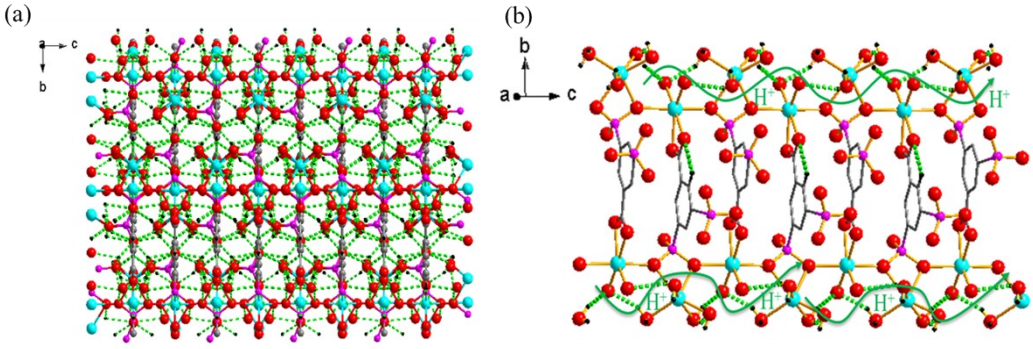

Figure S2. (a) Hydrogen bond network structure in Cd-MOF; (b) The proton transport path through hydrogen bond network in Cd-MOF.

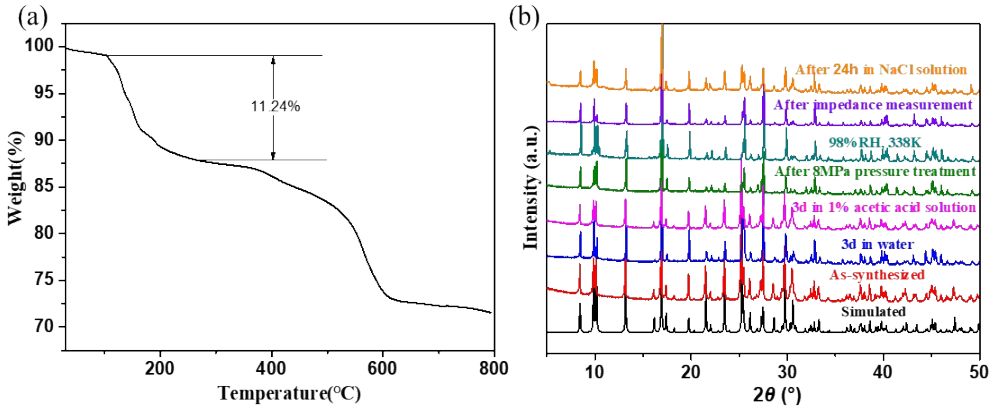

Figure S3. (a) The TGA of Cd-MOF; (b) The PXRD patterns of simulated and experimental for Cd-MOF.

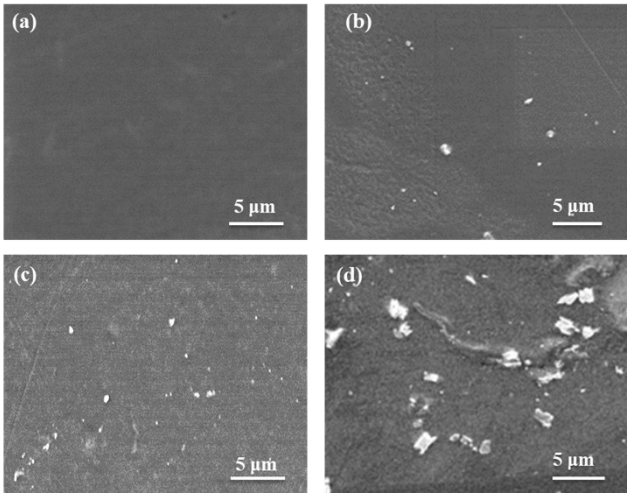

Figure S4. SEM images of composite membranes: (a) pure CS membrane; (b) Cd-MOF@CS-3; (c) Cd-MOF@CS-5; (d) Cd-MOF@CS-7.

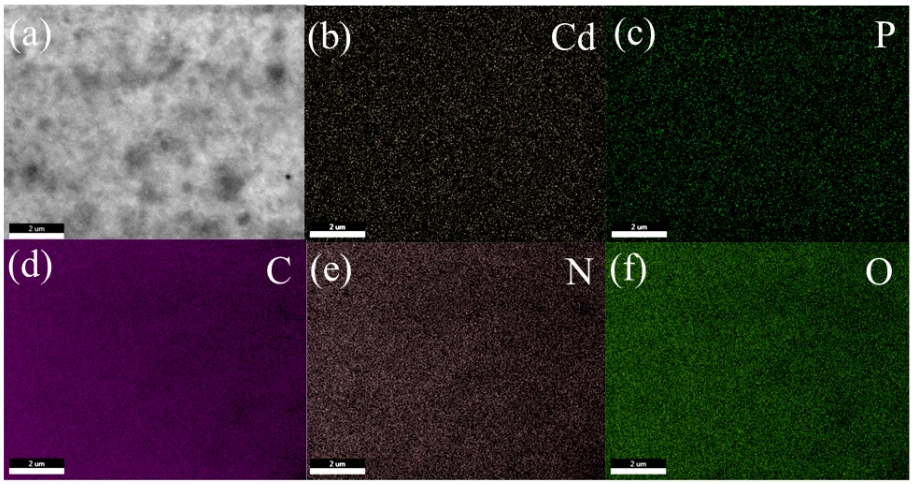

Figure S5. (a) SEM images of Cd-MOF@CS-5; (b-f) EDX elemental map of Cd, P, C, N, O in Cd-MOF@CS-5.

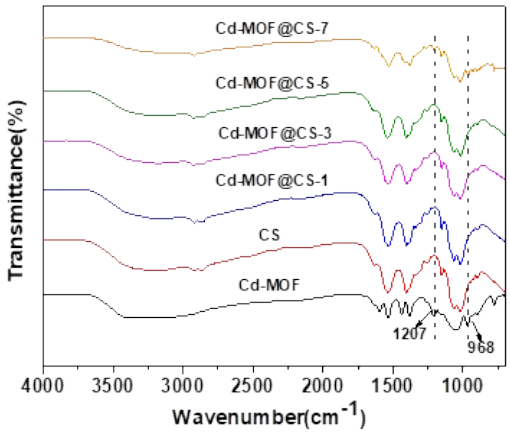

Figure S6. FT-IR spectra of Cd-MOF, pure CS membrane and Cd-MOF@CS-X (X=1%, 3%, 5%, 7% wt).

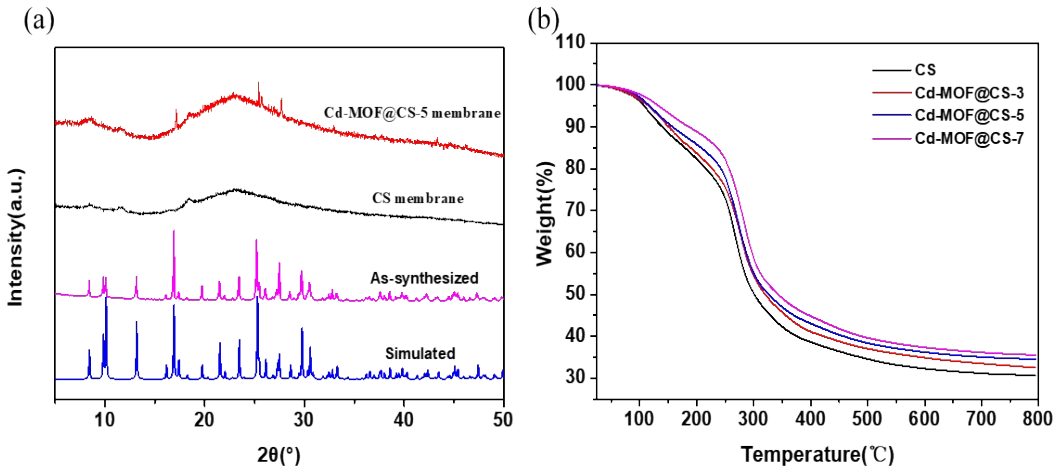

Figure S7. (a) PXRD patterns of Cd-MOF, pure CS membrane and Cd-MOF@CS-5 membrane; (b) TGA curves of pure CS and composite membranes.

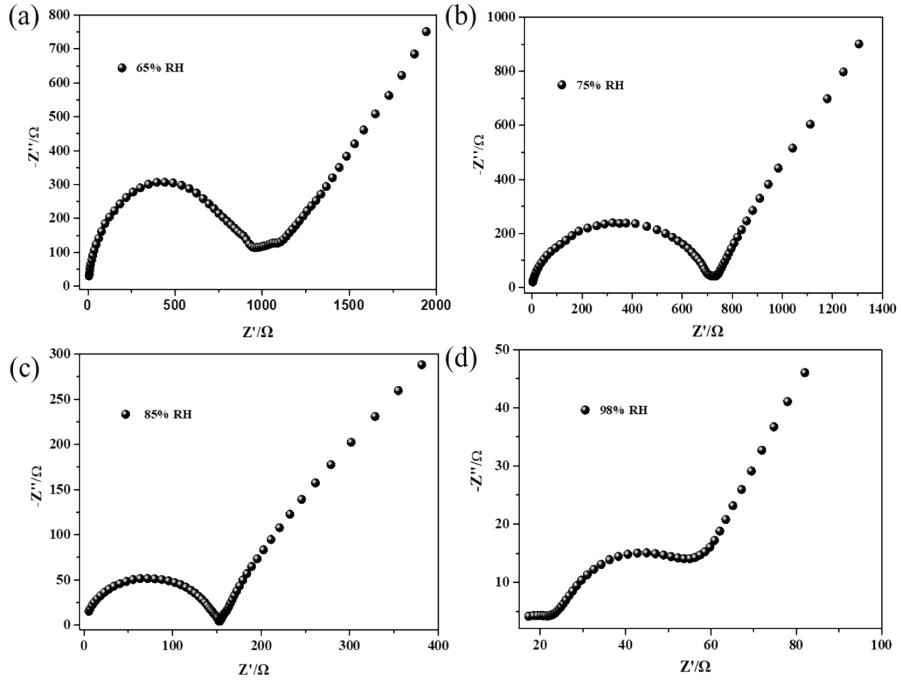

Figure S8. Nyquist curve of Cd-MOF under different relative humidity conditions at 298 K: (a) 65%RH; (b) 75%RH; (c) 85%RH; (d) 98%RH.

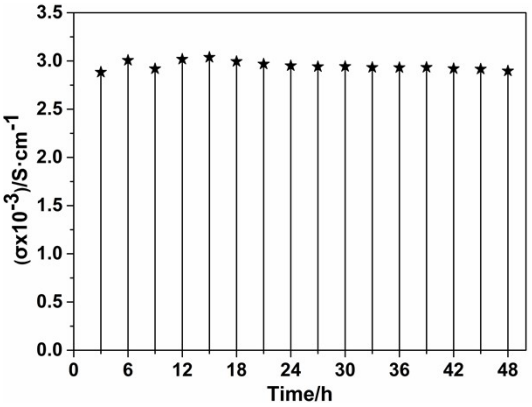

Figure S9. Time-dependent proton conductivity of Cd-MOF in proton conduction at 98% RH and 338 K.

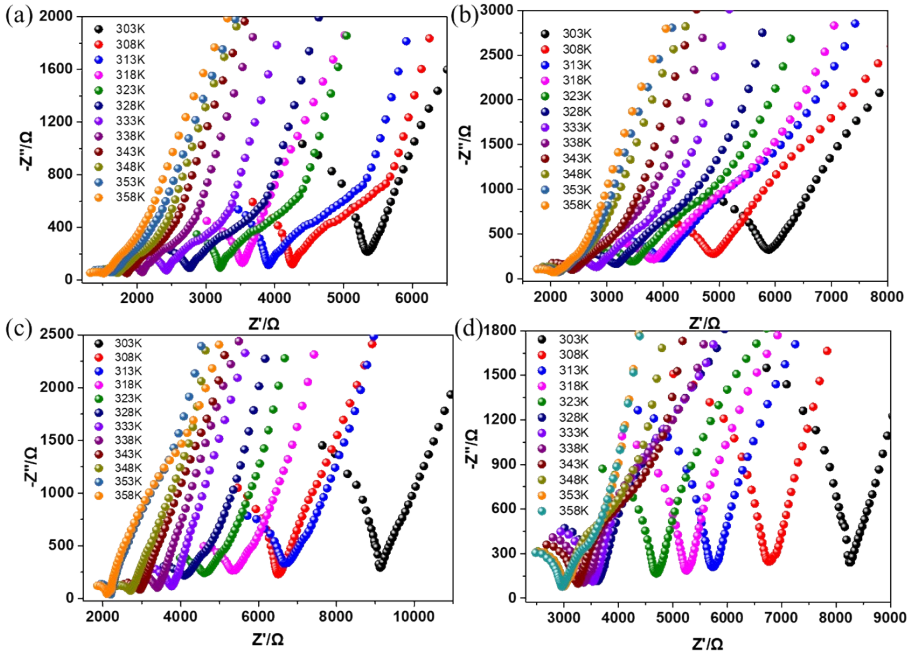

Figure S10. Temperature-dependent AC impedance diagram of composite membranes at 98%RH: (a) Cd-MOF@CS-1 (b) Cd-MOF@CS-3 (c) Cd-MOF@CS-5 (d) Cd-MOF@CS-7.

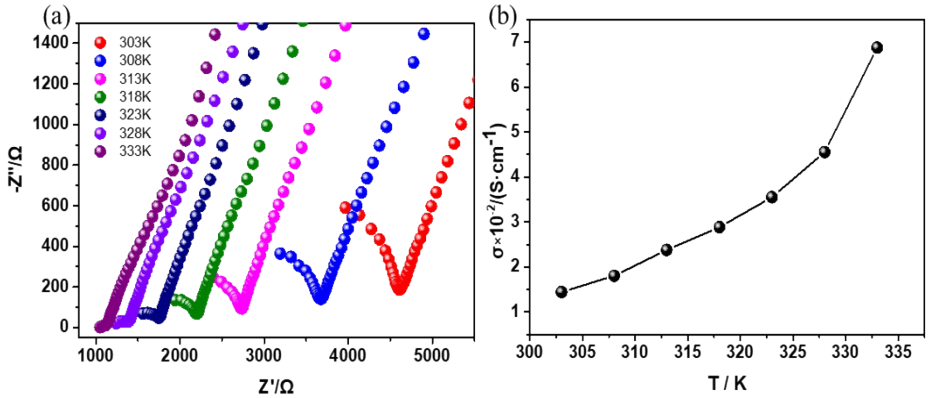

Figure S11. (a) Temperature-dependent impedance spectrum of the pure CS membrane; (b) The proton conductivity of the pure CS membrane changes with temperature at 98% RH.

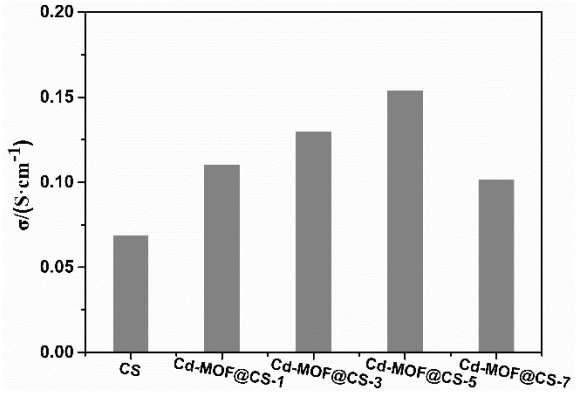

Figure S12. The proton conductivity of pure CS membrane and Cd-MOF@CS-X (X=1%, 3%, 5%, 7% wt) at 98% RH and 333K.

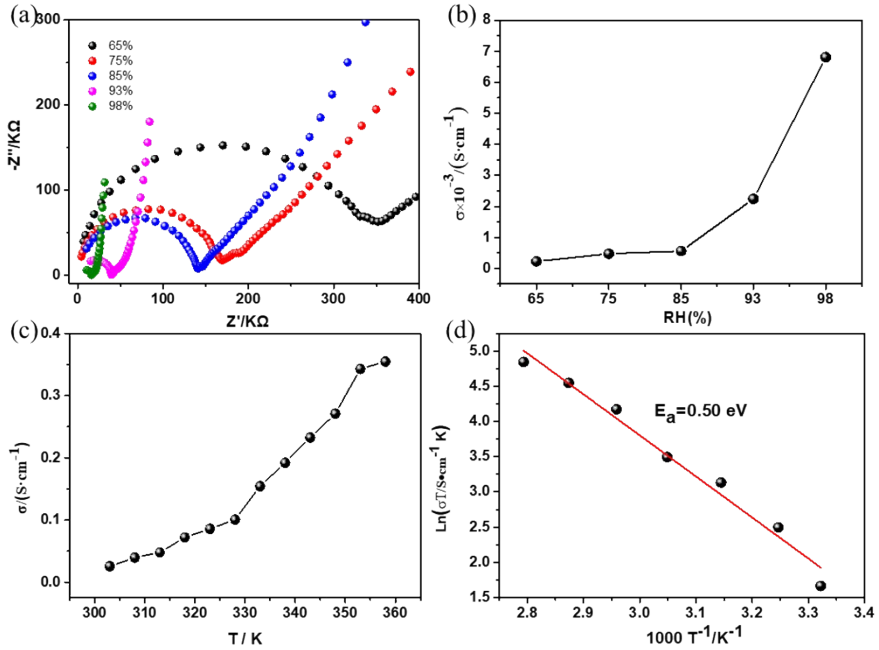

Figure S13. (a) Humidity-dependent impedance spectrum of the Cd-MOF@CS-5 membrane; (b) The relation curve between proton conductivity and relative humidity of Cd-MOF@CS-5 membrane at 298 K; (c) The proton conductivity of the Cd-MOF@CS-5 membrane changes with temperature at 98% RH; (d) Arrhenius plot for the activation energy of Cd-MOF@CS-5 membrane.

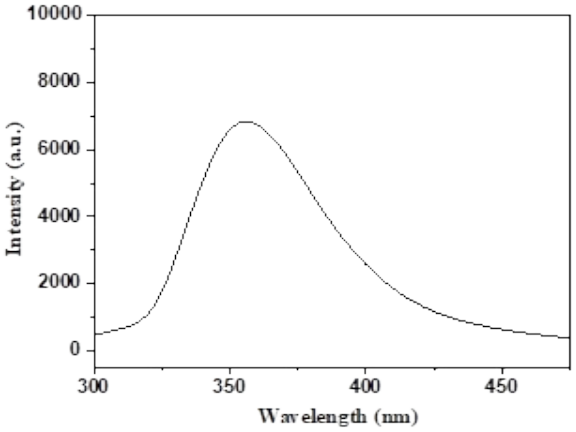

Figure S14. The emission spectrum of Cd-MOF in ethanol (λ_{ex}=265 nm).

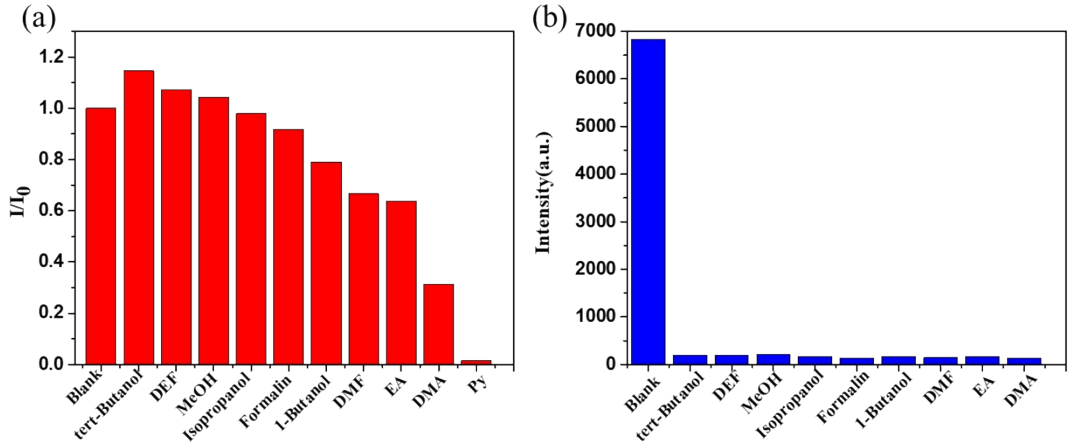

Figure S15. (a) The relative intensity ratio of Cd-MOF in different organic small molecule solvents upon excitation at 265 nm; (b) Fluorescence intensity of pyridine in various organic solvents excited at 365 nm.

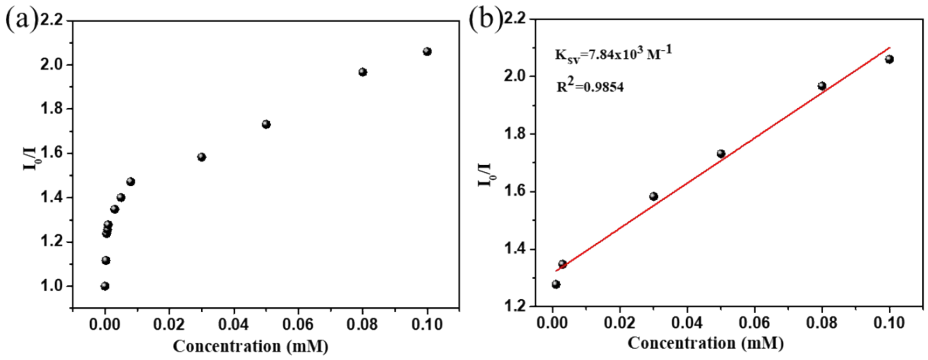

Figure S16. (a) The relationship between I_0/I and the concentration of pyridine solution (0~10^{-4} M); (b) The Stern-Volmer plot of I_0/I versus the concentration of pyridine solution (10^{-6}~10^{-4} M).

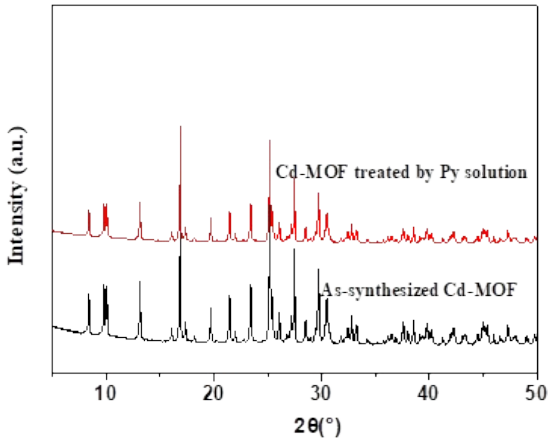

Figure S17. PXRD patterns of as-synthesized and Cd-MOF treated by Py solution.

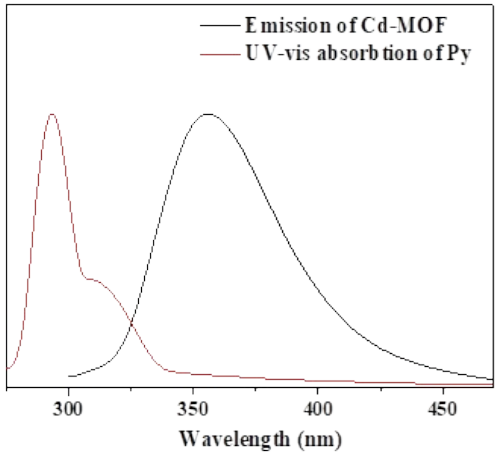

Figure S18. The emission spectra of Cd-MOF and the UV-vis absorption spectra of Py.

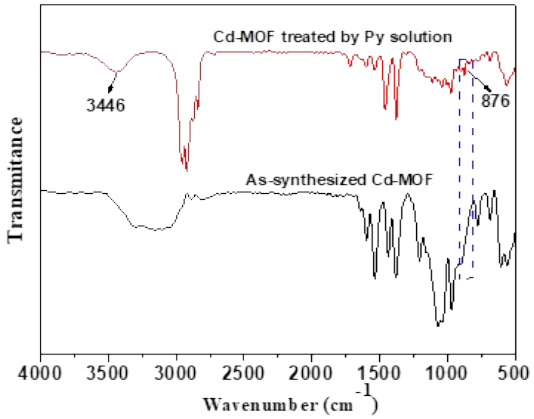

Figure S19. FT-IR spectra as-synthesized and Cd-MOF treated by Py solution.

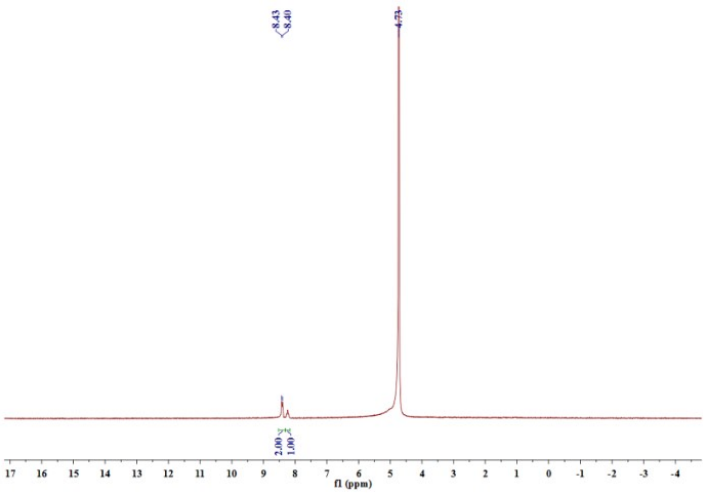

Figure S20. ^{1}H NMR spectra of H_5dpb.

References

1. V. Luca, J. J. Tejada, D. Vega, G. Arrachart and C. Rey, *Inorg Chem*, 2016, **55**, 7928-7943.
2. Y. Y. Cai, Q. Yang, Z. Y. Zhu, Q. H. Sun, A. M. Zhu, Q. G. Zhang and Q. L. Liu, *J. Membr. Sci.*, 2019, **590**, 117277.
3. L. Wang, N. Deng, G. Wang, J. Ju, B. Cheng and W. Kang, *ACS Appl Mater Interfaces*, 2019, **11**, 39979-39990.
4. Y. Guo, Z. Jiang, W. Ying, L. Chen, Y. Liu, X. Wang, Z.-J. Jiang, B. Chen and X. Peng, *Advanced Materials*, 2018, **30**.
5. F. Yang, G. Xu, Y. Dou, B. Wang, H. Zhang, H. Wu, W. Zhou, J.-R. Li and B. Chen, *Nature Energy*, 2017, **2**, 877-883.
6. X.-Y. Dong, J.-J. Li, Z. Han, P.-G. Duan, L.-K. Li and S.-Q. Zang, *Journal of Materials Chemistry A*, 2017, **5**, 3464-3474.
7. H. B. Luo, Q. Ren, P. Wang, J. Zhang, L. Wang and X. M. Ren, *ACS Appl Mater Interfaces*, 2019, **11**, 9164-9171.
8. X. Y. Dong, J. H. Wang, S. S. Liu, Z. Han, Q. J. Tang, F. F. Li and S. Q. Zang, *ACS Appl Mater Interfaces*, 2018, **10**, 38209-38216.